3D linear inversion of magnetic susceptibility data acquired by frequency domain EMI

J. Thiesson, Alain Tabbagh, F.-X. Simon, M. Dabas

3D linear inversion of magnetic susceptibility data acquired by frequency domain EMI

Thiesson[1] J., Tabbagh[1] A., Simon[2] F.-X., Dabas[3] M.

[1] Sorbonne Universités, UPMC Paris6, UMR7619, Métis, F-75252 Paris

[2] Institut National de Recherches en Archéologie Préventive, 121, rue d'Alésia, F-75000 Paris

[3] Geocarta, 5 rue de la banque F-75002 Paris

Abstract

Low induction number EMI instruments are able to simultaneously measure a soil's apparent magnetic susceptibility and electrical conductivity. This family of dual measurement instruments is highly useful for the analysis of soils and archaeological sites. However, the electromagnetic properties of soils are found to vary over considerably different ranges: whereas their electrical conductivity varies from ≤ 0.1 to ≥ 100 mSm^{-1}, their relative magnetic permeability remains within a very small range, between 1.0001 and 1.01 SI. Consequently, although apparent conductivity measurements need to be inverted using non-linear processes, the variations of the apparent magnetic susceptibility can be approximated through the use of linear processes, as in the case of the magnetic prospection technique.

Our proposed 3D inversion algorithm starts from apparent susceptibility data sets, acquired using different instruments over a given area. A reference vertical profile is defined by considering the mode of the vertical distributions of both the electrical resistivity and of the magnetic susceptibility. At each point of the mapped area, the reference vertical profile response is subtracted to obtain the apparent susceptibility variation dataset. A 2D horizontal Fourier transform is applied to these variation datasets and to the dipole (impulse) response of each instrument, a (vertical) 1D inversion is performed at each point in the spectral domain,

and finally the resulting dataset is inverse transformed to restore the apparent 3D susceptibility variations.

It has been shown that when applied to synthetic results, this method is able to correct the apparent deformations of a buried object resulting from the geometry of the instrument, and to restore reliable quantitative susceptibility contrasts. It also allows the thin layer solution, similar to that used in magnetic prospection, to be implemented. When applied to field data it initially delivers a level of contrast comparable to that obtained with a non-linear 3D inversion. Over four different sites, this method is able to produce, following an acceptably short computation time, realistic values for the lateral and vertical variations in susceptibility, which are significantly different to those given by a point-by-point 1D inversion.

Key-words: Magnetic susceptibility of soils, frequency domain EMI, 3D inversion of in-phase susceptibility measurements

Introduction

Soil is produced by various complex processes, to which human activities can make a significant contribution. A complete, continuous and non-invasive description of a soil's structure is thus of primary importance in terms of improving our knowledge of ancient societies, and ensuring more relevant management of the current environment. Geophysical surveys have thus been recognized as an indispensable tool for subsurface environmental studies (Butler 2005, Viscarra-Rossel et al. 2010). In addition to its electrical resistivity, the soil's magnetic properties have sufficient variability, and are sufficiently related to past and present active pedological processes (namely redox) (Evans and Heller 2003, Liu et al. 2012), to motivate their utilization in ground prospection campaigns. Magnetic prospection has been

51 the most commonly used technique in archeological applications (Aspinall et al. 2008), in
52 which spatial variations of the Earth's magnetic field, and thus all variations in the ground's
53 total magnetization, are measured. However, this technique fails to describe the vertical
54 layering of a terrain, and is thus less useful for pedological applications in which it is
55 important to identify the magnetic properties of each horizon; moreover, its ability to detect
56 lens-like features is very poor (Scollar et al. 1990). These limitations confirm the potential
57 usefulness of small, frequency-domain electromagnetic (also referred to as Slingram, loop-
58 loop, or dipole-dipole) instruments, which can simultaneously measure the ground's apparent
59 electrical conductivity and magnetic susceptibility (Parchas and Tabbagh 1978), and can now
60 be fitted with a multi-receiver capability (Saey et al. 2012, Bonsall et al. 2013).
61 The present paper focuses on the interpretation of measurements of the
62 ground's in-phase magnetic susceptibility. Other measurements, such as that of the ground's
63 magnetic viscosity (Thiesson et al. 2007), or measurements combining both EMI and the
64 magnetic technique, are reported to be highly advantageous in certain contexts (Benech et al.
65 2002, Pétronille et al. 2010). The aim of the present study is to assess the performance of a
66 fast 3D linear interpretation algorithm, which is easy to implement on a laptop computer.
67 Through the use of the Moment Method (MoM), fast 3D inversion processes have already
68 been proposed for DC resistivity prospection (Brinon et al. 2012), and for the simultaneous
69 interpretation of electrical conductivity and magnetic susceptibility EMI data (Benech et al.
70 2016), whilst this processes is limited to reduced areas in the vicinity of targeted features. In
71 the following, an inversion technique is proposed for the processing of magnetic susceptibility
72 variation data derived from the MoM. Since the relative magnetic permeability of the soil
73 varies only slightly (between 1.0001 and 1.01), it has been verified (Tabbagh 1985) that the
74 Born approximation can be applied to the analysis of such data, thus paving the way for the
75 use of linear inversion techniques: this is a sound approximation, and is systematically used in

magnetic prospection when the so-called demagnetizing field is neglected (Grant and West 1965, Scollar et al. 1990). On the other hand, it cannot be applied in the case of DC resistivity (Dabas et al. 1994, Buvat *et al.* 2013) or conductivity electromagnetic (EM) methods because the soil's electrical conductivity varies over a wide range, between ≤ 0.1 and ≥ 100 mS/m. The implementation of a linear method has the advantage of being more efficient computationally, thus allowing the entire surveyed surface to be processed in one go.

Our proposed interpretation process is divided into two phases. In the first of these, the usual 1D non-linear inversion scheme is applied, point by point, to determine the vertical distributions of both electrical conductivity and magnetic susceptibility (Zhang and Oldenburg 1999). These vertical distributions are often sufficient to allow the terrain's structure to be characterized. If marked lateral changes require a 3D inversion the statistical mode of these distributions as a function of depth is taken to be the reference vertical profile. Then, during the second phase, the interpreter determines the lateral variations in susceptibility with respect to this profile. Since the response of a contrasting magnetic body can be assumed to be linear, this process involves successively applying a 2D (horizontal plane) Fourier transform, non-linearly inverting the resulting spectrum of the 1D vertical distribution of magnetic susceptibility contrasting with respect to the reference profile, and finally computing the lateral susceptibility contrast variations by means of an inverse Fourier transform. The full process is illustrated in Figure 1.

Reminder of the 1D inversion process

The EMI instruments under consideration have a transmitting coil and at least one receiving coil at a metric separation expressed by L. The coils are located at a height d, above ground level. The coil orientations can be adjusted, and various possible configurations have been defined (Frischknecht et al. 1991) with respect to the plane of the coils. The most

commonly used configurations are HCP (horizontal coplanar), VCP (vertical coplanar), PARA (parallel – inclined at 55° from the horizontal plane), and PERP (perpendicular). The application of the instrument's primary field over a layered ground generates complex secondary fields, H_s, which are expressed by Hankel Transform integrals. The full development of these expressions, and the definition of the subsequent approximations are described by Thiesson et al. (2014). The method used to compute these transforms (i.e. the forward problem) is well known, and is similar to that used for vertical electrical sounding (Ghosh 1971). The calculation results can be expressed in terms of apparent properties, this allows an initial approximate evaluation to be made of the soil's properties, thus simplifying comparisons between different instruments. The apparent magnetic susceptibility, κ_a, is the susceptibility of a homogeneous terrain that would produce the same results with the same instrumental geometry (L, coil orientation, height above the surface).

The inverse problem is usually solved by starting from an *a priori* guess at the values of the unknown parameters, which are iteratively modified until a good fit between the computed results and the apparent experimental properties is reached. The number of parameters is limited by the number of different geometrical configurations which can be adopted by the instrument (coil orientations and L distances), since at the studied frequencies (VLF and LF) and depth ranges, the investigation depth is governed by the instrument geometry. Although a single parameter inversion can sometimes be useful (Guerin et al. 1996), several instruments (or a multi-coil configuration in the same apparatus) clearly provide a more detailed description of the terrain's structure.

It is important to note that with EMI data inversion, the vertical conductivity profile must first be determined (using the quadrature out of phase component of the responses), prior to inversion of the magnetic susceptibility profile because: (1) the conductivity distribution modifies the total magnetic field distribution in the ground, whereas the terrain's

vertical susceptibility distribution has a negligible influence on the total magnetic field distribution (Tabbagh 1985) and (2) when high, the conductivity may generate an in-phase response (Thiesson et al. 2014) that must be subtracted from the total in-phase response.

At the end of the 1D inversion step, the statistical mode of each model parameter is adopted, in order to define the reference vertical profile. A susceptibility response $\kappa_{a0}(d)$ is associated with this profile, and is subtracted from the experimental response at each point *(x, y)* of the surveyed area, and for each receiver (at elevation *d*), thereby defining a contrasting magnetic susceptibility response $\delta\kappa_a(x, y, d)$.

2D (x,y) inversion using a Fourier transform

Principle

Given $\delta\kappa(x',y',z')$, the contrasting magnetic susceptibility distribution inside the ground, and since the problem to be solved is linear, the response $\delta\kappa_a(x, y, d)$ that is added to the response of the reference profile can be expressed as a convolution product:

$$\delta\kappa_a(x, y, d) = \iiint_{\infty} \delta\kappa(x', y', z')\, IR(x - x', y - y', d - z')\, dx'\, dy'\, dz' \qquad (1),$$

where *IR* is the 'impulse response', the 3D Green function corresponding to the dipole source response to the instrumental configuration under consideration (analytical expressions corresponding to these functions are presented in more detail in (Tabbagh 1985)). If the ground is discretized in the form of *N* successive layers having thicknesses e_i centered at z_i, and a magnetic susceptibility contrast $\delta\kappa(x', y', z_i)$, equation (1) can be approximated by:

$$\delta\kappa_a(x, y, d) = \sum_{i=1}^{N} e_i \iint_{\infty} \delta\kappa(x', y', z_i)\, IR(x - x', y - y', d - z_i)\, dx'\, dy' \qquad (2).$$

By applying a 2D Fourier transform to Eq. (2) one has:

$$\delta\hat{\kappa}_a(u, v, d) = \sum_{i=1}^{N} e_i\, \delta\hat{\kappa}(u, v, z_i)\, \hat{IR}(u, v, d - z_i) \qquad (3),$$

where a 'circumflex accent' indicates Fourier transformed functions, and *(u, v)* are the spatial frequencies corresponding to *(x, y)*. Consequently, at each point *(u, v)* the expression for Eq. (3) corresponding to each level z_i can be thought of as a single component of an *N*-equation linear system. If the number of different geometric coil configurations *K* is smaller than *N,* the system has no solution, however when $K = N$ it can be solved directly. When $K > N$ the system can be solved using the least squares method. Knowing $\delta\kappa(u, v, z_i)$, it is straightforward to derive the solution for the problem of 3D susceptibility contrast via the inverse transformation of $\delta\hat{\kappa}(x, y, z_i)$.

The thin layer solution

Although commercial multi-configuration instruments are now commonly available and used in field surveys, a considerable volume of data has been acquired over the last forty years using just one type of configuration. It is thus important to reconsider and enhance the interpretation of this data. When a single configuration is used, only one layer can be considered and the resulting thin-layer interpretation is similar to that obtained with potential methods (Grant and West 1965). In the case of magnetic prospection, this is a valuable solution (Desvignes et al. 1999) since it allows: (i) the general pattern of the source body to be restored by correcting for the influence of the Earth's magnetic inclination on the shape of the anomaly; (ii) the maximum source depth to be assessed, and (iii) the magnetization contrast to be determined. Similar issues arise when interpreting EMI apparent magnetic susceptibility data: deformations introduced by the coil configuration, poor accuracy of depth assessments, and the contrast of any source body. This similarity has made it possible to use transformations between apparent susceptibility measurements and induced magnetization anomalies of the Earth's magnetic field, and has opened up significant perspectives for the simultaneous interpretation of both types of data (Benech et al. 2002). In the present study,

174 our analysis is limited to that of EMI measurements, for which the determination of the depth
175 of the thin layer raises a specific issue: a relationship clearly does exist between the coil
176 separation and the depth at which a susceptibility variation can be detected, if the sensitivity at
177 a depth is too low, then the inversion near that depth will be poor.

178 We thus consider a series of synthetic cases, in which a 2m x 2m slab with a thickness
179 of 0.2 m and susceptibility contrast equal to 200 10^{-5} SI is displaced along the vertical axis.
180 The apparent susceptibility maps are inverted for each different position (change in depth) of
181 the slab, and the quality of the inversion is assessed by comparing the susceptibility contrast
182 produced by the inversion with the original value. Table 1(a) presents the results obtained for
183 the different depths of the slab and coil separations using VCP configuration. Table 1(b)
184 provides the results with the PERP configuration, Table 1(c) the results with the HCP
185 configuration, Table 1(d) the results with the PARA configuration. Four main conclusions can
186 be drawn for these comparisons:

187 (1) With the VCP configuration, the slab is correctly restored, even for a coil
188 separation of L=2m and shallow slab depths, as well as for smaller coil separations and
189 greater depths.

190 (2) With the PERP configuration, the results are comparable to those for the VCP
191 configuration, and (with the exception of shallow slabs with VCP) the inverted values are
192 generally 10% to 20% higher than the original values. For shallower slabs the outcome can
193 probably be explained by the more complex lateral variations of the PERP dipole impulse
194 response, and thus more problematic inversion of PERP data.

195 (3) With the HCP and PARA configurations the sign of the contrast is correctly
196 restored (the apparent susceptibility anomaly is negative for greater d/L ratios with HCP) but
197 not its magnitude (most often significantly amplified)

198 (4) This preceding example, established using synthetic data, shows that good depths
199 of investigation can be reached, even for the case of smaller values of *L*.
200 However, even for one thin layer, the simultaneous use of several configurations leads
201 to slightly better results than the use of a single configuration.
202
203 ***Multi-layer inversion***
204 At each point of the spectral domain, the solution $\delta\kappa(u,v,z_i)$ is represented by an *N*
205 component vector $\delta\vec{\kappa} = (\kappa_1,...,\kappa_N)$, the solution for the linear equation system. While in
206 practice limited to few components, the solution for the *N* linear equations system is
207 confronted by an instability arising from the fact that an abnormal value in one layer can be
208 compensated by another abnormal value, of the opposite sign, in another layer. The solution
209 can be stabilized by adding an external constraint, for example by minimizing the norm of the
210 solution vector. Although it is also possible to use this constraint to introduce the depth
211 sensitivity dependence associated with each coil configuration, this sensitivity tends to be of
212 the 'all or nothing' type, as shown in Table 1. Following several tests, two options were found
213 to be potentially useful: either minimizing the square of the norm of the $\delta\vec{\kappa}$ vector (constraint
214 I):

215 $$Q = \sum_1^N \hat{\kappa}_i^2 , \qquad (4),$$

216 or minimizing the sum of the squares of the differences between consecutive components
217 (constraint II):

218 $$Q = \sum_2^N (\hat{\kappa}_i - \hat{\kappa}_{i-1})^2 \qquad (5).$$

219 Thus, for *K* different instruments the minimized quantity is:

220 $$\sum_{j=1}^{K} (\delta\hat{\kappa}_{a,\exp,j} - \delta\hat{\kappa}_{a,theo,j})^2 + \lambda Q \qquad (6),$$

where λ is chosen by the interpreter: for the second option the value $\lambda=1$ would be set, whereas with the first option it is more convenient to use the trace of the Jacobian matrix: $\lambda = trace/2$. With constraint II the stabilization is stronger, the vertical variation of the magnetic susceptibility contrast minimum.

The application of this inversion procedure using synthetic data computed for PERP, VCP and PARA configurations and inter-coil distances varying between 0.7 and 1.5 m is presented in Table 2 for the case of constraint II and for λ=1. The body is 2m x 2m x 0.6m sized, it presents a 200 10^{-5} SI susceptibility contrast, it is centered at z=0.5 m and divided in 5 layers (0.12m thick). Equivalently good results were obtained with reduced number of layers equal to: 3 (0.2 m thickness) or 4 (0.15 m thickness).

Tests with multi-body synthetic data

We consider a rectangular 25 m x 17 m area, meshed onto a regular 0.5m x 0.5m grid, containing four different magnetic bodies (Fig. 2) imbedded in a terrain with a homogeneous resistivity equal to 70 Ωm, and susceptibility equal to 30 10^{-5} SI. The first body (A) is an L-shaped ditch with a 1m x 0.4 m cross section, centered at a depth of 0.4 m, the two perpendicular branches of which are 8 m in length and have a susceptibility contrast of 120 10^{-5} SI. The second body (B) is a medium-sized square body with dimensions 2m x 2m x 0.75 m, centered at a depth of 0.6 m and having a susceptibility contrast equal to 100 10^{-5} SI. The third body (C) is a small superficial feature with dimensions 0.4m x 0.4m x 0.2 m, centered at a depth of 0.3 m depth and having a susceptibility contrast equal to 100 10^{-5} SI. The fourth body (D) is a slim feature with dimensions 0.4m x 0.4m x 1.6 m, centered at a depth of 1 m and having a susceptibility contrast equal to 100 10^{-5} SI. The apparent magnetic susceptibility maps computed using MoM are shown in Fig. 3, for the seven different apparatus geometries described in Table 3. For all configurations, the transmitter–receiver

line lies parallel to the x axis. The four features, with their different geometries, can be recognized in each map. These are characterized by ringing, especially in the case of the longest coil separations. It should be noted that the shortest apparatus provides the best description of the four magnetic bodies, in terms of the shape and the magnitude of the associated anomalies.

The seven datasets were inverted together, whilst considering three layers with different values of magnetic susceptibility, the first centered at z_1=0.3 m with a thickness e_1=0.2 m, the second centered at z_2=0.5 m with a thickness e_2=0.2 m, and the third centered at z_3=0.8 m with a thickness e_3=0.4 m. When 1D inversion is applied (Fig. 4), although the four features are correctly identified, this inversion fails to correct for their deformed shapes and for the apparent anisotropy, produced by the different coil orientations. This issue is particularly pronounced for small features, whose precise locations are difficult to restore. In addition, ringing with sign changes cannot be eliminated, and is even amplified in the third layer in which there should be no variations corresponding to the superficial features (A) and (C). These spurious variations are a consequence of the instrument's low sensitivity to 3D changes at the depth of these features.

The results produced by 3D linear inversion are presented in Fig. 5, showing that the body's shapes are faithfully restored, and the susceptibility values are in good agreement with the original values for the first two layers. However, in the case of feature (A) the third layer is again characterized by greater amplitude variations, resulting from the fact that the instruments' sensitivities are too low to constrain the solution.

Interpretation of field data

In order to assess the potential of this approach for data inversion under field conditions, we analyzed the data acquired using various instrument geometries, at four

different archaeological sites characterized by different climatic conditions and soil environments. In all cases we started from the apparent susceptibility data sets which have been obtained after checking the instrument calibration (Thiesson et al. 2014) and transforming the in-phase secondary field measurements. Where the electrical conductivity is high (Medamud case), the apparent electrical conductivity was first determined using the quadrature response and then used to calculate the in-phase response which was algebraically subtracted from the total in-phase response.

Neolithic enclosure at Balloy (Seine et Marne, France)

The eastern section of this middle-neolithic 'Passy' type of funeral enclosure (Mordant 1997) has been the object of multi-method tests. This enclosure was detected using both electrical (1 m square array) and SH3 prospection (see appendix 1 for the characteristics of the latter device), but was not detected by magnetic prospection using a fluxgate gradiometer with 1 nTm^{-1} sensitivity (Hesse 1987). This failure was explained by the use of a 3D non-linear inversion (Bénech *et al*. 2016), applied to a selected zone (indicated by a rectangular outline in Fig. 6), showing that the SH3 measurements had revealed a 1.4m x 0.4 m cross-sectional feature, surrounded by gravel, with magnetic susceptibilities of respectively 51 x 10^{-5} and 20 x 10^{-5} SI. Using these parameters, the induced magnetization anomaly determined for a fluxgate vertical gradiometer is less than 0.5 nTm^{-1}, and even with the addition of viscous magnetic remanent magnetization the anomaly cannot clearly overpass $1nTm^{-1}$.

In the present study we consider just one layer (since only one instrumental dataset was recorded), of 0.4m thickness and centred at a depth of 0.45m. For the same selected zone, the following results are obtained:

(1) as could be expected, the 1D inversion produces the same image as that generated using the apparent susceptibility measurements (Fig. 6b),

(2) the susceptibility variations are in agreement with the 3D non-linear inversion, with a magnetic susceptibility of 40 10^{-5} SI for the ditch filling, in contrast with a value of 10 x 10^{-5} SI for the immediately surrounding gravel. This calculation was made for the totality of the 26m x 26 m surface shown in Fig. 6, and required just 7s of computing time, whilst using the same laptop computer (4 Go RAM, 2.5 GHz) the non-linear inversion over the 2.5m x 5m area required 267s of computing time.

Neolithic settlement of Perdika 2 (Central Greece)

This neolithic settlement, in this region referred to as a *magoula*, is located on the eastern Thessalian plain of Greece and was surveyed using different methods in the frame of the IGEAN project (Innovative Geophysical Approach for the study of Early Agriculture villages of Neolithic Thessaly) (Simon et al., 2015). The magnetic survey revealed a complex system of enclosures (Fig. 7). In order to acquire a better description of what is thought to be an enclosure entrance, a 40m x 40m area was prospected using the CMD instrument (see Appendix I for its characteristics). The ditches are more clearly discernible by their magnetic susceptibility contrast than by their electrical conductivity. The resistivity variations are relatively small, lying within a moderate range of values: a 150 Ωm layer of topsoil, and subsoil variations ranging between 30 and 100 Ωm. As the magnetic susceptibility data acquired with the shorter coil separation (L=0.32m) was too noisy for suitable interpretation, we made use of four data sets for the inversion (Fig. 8): HCP with 0.71 m and 1.18 m separations, and VCP with 0.71 m and 1.18 m separations. The topsoil layer was assumed to be homogeneous. In order to assess the vertical extent of the archaeological features, we chose to divide the subsoil into two contiguous layers of 0.5 m thickness, with the first lying between 0.2 and 0.7 m, and the second between 0.7 and 1.2 m. The images produced by point-by-point 1D inversion and by 3D linear inversion of the data are presented in Figs. 9a

and 9b, respectively. In the 1D inversion, the second layer reveals some features that are different to those found in the first layer, which is characterised by strong susceptibility variations. Also performed using constraint I, see equation (4), the 3D linear inversion shows that the ditches are shallow, and that different features appear at greater depths, but with smaller variations in susceptibility.

Middle Kingdom Kôm of Medamud (Egypt)

The site of Medamud is located 4 km to the north of Karnak, and was occupied for a long period of time, from the Middle Kingdom of Egypt until the Roman era (Relats-Montserrat 2016(a)). The geophysical survey initiated by the IFAO tended to characterize a Middle Kingdom pottery workshop area. The survey was carried out with the CMD (see Appendix I) instrument in a VCP configuration, in order to simultaneously describe the soil's electrical conductivity and magnetic susceptibility. In the area under consideration the fine-grained, thick archaeological layer present just below the surface has a very low resistivity, centred on 16 Ωm, for which a correction is required to eliminate the in-phase component of the conductivity response

In the present study we consider a 44m x 60m zone from this site. Fig. 10 shows three apparent susceptibility maps, produced using inter-coil distances of 0.32, 0.71 and 1.18 m, respectively. Fig. 11 shows the results of the inversions when two layers are considered, with the first situated between 0.05 and 0.35 cm, and the second between 0.35 and 0.65 m: Fig. 11a and Fig. 11b show the results of the 1D and 3D inversions (both using constraint I), respectively. Both inversions show that the magnetic features have a significant vertical extent (which probably exceeds the range of the instrument), and that their susceptibilities are high. However, comparisons between these different results underscore the fact that when 1D inversion is used, the second layer has higher values, in the range [350 – 1250] 10^{-5} SI,

346 whereas the first layer remains close to a modal value of 200 10^{-5} SI, which is the same as that
347 found for both layers with the 3D inversion. Again in this case, the second layer of the 3D
348 inversion is characterised by a narrower range of variations ([180 – 225] 10^{-5} SI) than the first
349 layer ([130 – 330] 10^{-5} SI).

350 These maps clearly show the presence of a mud brick wall which corresponds to lower
351 apparent susceptibilities. By comparing these results with measurements (MS2D Bartington
352 Ltd) taken over another feature we obtain values in the range [60 – 90] 10^{-5} SI for the mud
353 bricks and a modal value of 178 10^{-5} SI for the surrounding magnetic soil (Relats-Montserrat
354 et al. 2016(b)). When applying a full 3D inversion to the rectangular 12m x 3 m area (marked
355 in Figure 11b) we obtain, by considering a wall of 0.6m thickness and 4m width, a
356 susceptibility contrast of -92 10^{-5} SI with the surrounding soil. These results are in fair
357 agreement with the results mapped in Figure 10b and with the 3D linear inversion using one
358 layer of 0.6m thickness which gives a -100 10^{-5} SI susceptibility contrast.

359

360 ***Destroyed medieval city of Thérouanne (Pas-de-Calais, France)***

361 Thérouanne was originally a Gallic, then an important Gallo-roman city, and during
362 medieval times was one of the main centres of the Picardie region in France. In 1553 it was
363 besieged and totally levelled by Charles Quint. This location was settled again as a small
364 village, only at the end of the XIXth century. The aim of the survey was to identify the
365 remains of the ancient medieval city, through a series of EMI and electrical prospection
366 campaigns. The test area considered here covers a surface area of 180m x 40m, and was
367 surveyed using the DualEM instrument (see Appendix I) in both HCP and VCP base
368 configurations. From this archaeological survey, we produced six different apparent magnetic
369 susceptibility maps, derived from the instrument's in-phase recordings made with the HCP
370 1m, HCP 2m, PERP 1.1m, PERP 2.1m, VCP 1m and VCP 2m configurations. In the present

371 analysis, the longest inter-coil separations of 4 m and 4.1m were not used, and the HCP 1m
372 and PERP 2m channels produced corrupted data. Thus, only four independent magnetic
373 susceptibility maps could be used, as shown in Fig. 12.

374 The electrical resistivity maps of the terrain reveal a 70 Ω m topsoil layer, followed by
375 a conductive subsoil layer with a resistivity between 10 and 60 Ωm, suggesting a significant
376 clay content (the salt spread under the order of Charles Quint was probably leached out well
377 before the time of the prospection campaign). The apparent magnetic susceptibility is
378 generally high, and higher for the PERP 1m and HCP 2m measurements than for both VCP
379 configurations (different susceptibility scales are used in Fig. 12). The change in sign of the
380 susceptibility response for the HCP 2m measurement, at approximately 0.75m, suggests that
381 most of the observed features have shallow locations. Three layers were considered for the
382 inversions: the first between 0.25 and 0.75 m; the second between 0.75 and 1.25 m; and the
383 third between 1.25 and 2.25 m. The results of the 1D point-by-point inversion are presented in
384 Fig. 13, and those of the 3D linear inversion are shown in Fig. 14. Constraint I was applied for
385 both inversions. Although the mean values of susceptibility decrease slightly with depth in the
386 1D inversion, the lateral variations have the same aspect and reproduce those of the four
387 apparent susceptibility maps. A large, 40 m diameter semi-circular feature, centred 18m to the
388 north of the image centre, can be seen in all three layers, thus suggesting that it has a
389 substantial vertical extent. In the 3D inversion, the first layer is clearly more magnetic than
390 the remaining two layers (the scales are different in Fig. 14), and the large semi-circular
391 feature is less noticeable in the deepest layer.

392

393 **Conclusion**

394 The new linear inversion technique presented here has been tested on synthetic and
395 field data. When compared with the original model, or with the complete 3D MoM inversion

technique, it provides reliable results for the shape of the sought features, as well as the magnitude of the contrasts. It is shown to be highly efficient for the correction of anomalous deformations, caused by the instrument's geometry, of a feature's geometrical outlines. By using the instrument's dipole impulse response in the analysis, this technique takes the influence of the real instrumental geometry into account, including that of the coil orientations. Its results are thus significantly different to those obtained with 1D point-to-point inversions, in terms of susceptibility variations as a function of depth, making it possible to improve the identification of the vertical boundaries of a given feature.

It should be underlined, however, that this technique is limited by the number of different available instrument geometries: in practice the magnetic susceptibility contrasts of only a rather small number of layers at a limited number of depths can be inversed. It is very valuable to have even this limited information on depth and susceptibility and where necessary the prospector has the possibility to increase the number of instruments geometries by considering measurements acquired at several altitudes with the same device.

Compared to 3D complete MoM inversion, the rapidity of this technique not only leads to a significant gain in time, but also provides the interpreter with the ability to test several stabilization process options, such as the choice of the number of layers or layer thicknesses. This also makes it possible to assess the probable vertical extent of the different features, through the use of a vertically translated thin layer.

References

Aspinall A., Gaffney C., Schmidt A., 2008. Magnetometry for archaeologists, Altamira Press, Lanham, 208 p.

Benech C., Dabas M., Simon F.-X., Tabbagh A., Thiesson J., 2016. Interpretation of shallow EMI resistivity and magnetic susceptibility measurements using rapid 1D/3D inversion. Geophysics, 81-2:E103-112. doi.org/10.1190/geo2014-0549.1.

Benech C., Tabbagh A.; Desvignes G., 2002. Joint interpretation of E. M. and magnetic data for near-surface studies. Geophysics, 67-6: 1729-1739.

Bonsall J., Fry R., Gaffney C., Armit I., Beck A., Gaffney V., 2013. Assessment of the CMD Mini-Explorer, a new low-frequency multi-coil electromagnetic device, for archaeological investigations. Archaeological Prospection 20: 219-231.

Brinon C., Simon F. X., Tabbagh A., 2012. Rapid 1D/3D inversion of shallow resistivity multipole data: examples in archaeological prospection. Geophysics, 77-3: E193-E201.

Butler D. K., 2005, Near Surface Geophysics (Investigations in Geophysics), Society of exploration geophysicists, Tulsa OK USA, 732 p.

Buvat S., Schamper C., Tabbagh A., 2013. Approximate 3D resistivity modelling using Fourier analysis of layer resistivity in shallow soil studies, Geophysical Journal International, 194-1: 158-169.

Dabas M., Tabbagh A., Tabbagh J., 1994. 3-D inversion in subsurface electrical surveying-I: Theory. Geophysical Journal International, 119, 975-990.

Desvignes G., Tabbagh A., Benech C., 1999. About the determination of magnetic anomaly sources. Archaeological Prospection, 6-2: 85-105.

Evans M., Heller F., 2003. Environmental Magnetism, Principles and Applications of Enviromagnetics. Academic Press, 295p.

442 Frischknecht F. C., Labson V. F., Spies B. R., Anderson W. L., 1991. Profiling methods using
443 small sources. In Electromagnetic methods in applied geophysics, volume2, applications, part
444 A, edited by M. N. Nabighian, SEG, Tusla OK, 105-252.
445 Ghosh D. P., 1971. The application of linear filter theory to the direct interpretation of
446 geoelectrical resistivity sounding measurements. Geophysical Prospecting, 19-2: 192-217.
447 Grant F. S., West G. F., 1965. Interpretation theory in applied geophysics, McGraw-Hill,
448 583p.
449 Guérin R., Méhéni Y., Rakontodrasoa G., Tabbagh A., 1996. Interpretation of Slingram
450 conductivity mapping in near surface geophysics: using a single parameter fitting with 1D
451 model. Geophysical Prospecting, 44-2: 233-249.
452 Hesse A., 1987, Balloy 1986-1987. Rapport de synthèse sur les prospections géophysiques
453 des vestiges archéologiques: Direction régionale des antiquités d'Ile de France, août 1987,
454 15p.
455 Liu Q., Roberts A. P., Larrasoana J. C., Banerjee S. K., Guyodo Y., Tauxe L. Oldfield F.,
456 2012, Environmental magnetism, Principle and applications. Review of Geophysics, 50: 1-50.
457 Mordant D., 1997, Le complexe des Réaudins à Balloy: enceinte et nécropole monumentale.
458 La Culture de Cerny. Nouvelle économie, nouvelle société au Néolithique : Actes du
459 Colloque International de Nemours 1994, Mémoires du Musée de Préhistoire d'Ile-de-France,
460 6, 449-479.
461 Parchas C., Tabbagh A.; 1978. Simultaneous measurement of electrical conductivity and
462 magnetic susceptibility of ground in electromagnetic prospecting. Archaeo-Physika, 10: 682-
463 691.
464 Pétronille M., Thiesson J., Simon F.-X., Buchsenschutz O., 2010. Magnetic signal
465 prospecting using multiparameter measurements : the case study of the Gallic site of Levroux.
466 Archaeological Prospection, 17-3: 141-150.

467 Relats-Montserrat F., 2016(a). Medamoud and the Nile: some preliminary reflections. In H.
468 Willems (ed.) The Nile: a natural and cultural landscape Mainzer Historische
469 Kulturwissenschaften in press.
470 Relats-Montserrat F., Thiesson J., Barahona Mendieta Z., Sanchez C., Réjiba F., Guérin R.,
471 2016(b). Une première campagne de prospection à Medamoud : la réouverture du chantier
472 (mission IFAO/Paris Sorbonne/Labex Resmed. Bulletin de l'Institut Français d'Archéologie
473 Orientale. Submitted
474 Saey T., De Smedt P., Meerschman E., Islam M-M., Meeuws F., van De Vijver E., Lehouck
475 A., van Meirvenne M., 2012. Electrical conductivity depth modelling with a multi-receiver
476 EMI sensor for prospecting archaeological features: Archaeological Prospection, 19-1: 21-30.
477 Scollar I., Tabbagh A., Hesse A., Herzog I., 1990, Archaeological prospection and remote
478 sensing. Cambridge University Press, 674p.
479 Simon F.-X., Kalayci T., Donati J.-C., Cuenca Garcia C. Manataki M., Sarris A., 2015. How
480 efficient is an integrative approach in archaeological geophysics, Comparative case studies
481 from neolithic settlements in Thessaly (central Greece). Near Surface Geophysics 13: 633-
482 643.
483 Tabbagh A., 1985. The response of a tree dimensional magnetic and conductive body in
484 shallow depth E.M. prospecting. Geophysical Journal of the. Royal Astronomical Society, 81-
485 1: 215-230
486 Thiesson J., Kessouri P., Schamper C., Tabbagh A., 2014. Calibration of frequency domain
487 electromagnetic devices used in near surface surveying: Near Surface Geophysics, 12, 481–
488 491.
489 Thiesson J., Tabbagh A., Flageul S., 2007. TDEM magnetic viscosity prospecting using
490 Slingram coil configuration. Near Surface Geophysics, 5-6: 363-374.

491 Viscarra Rossel, R. A., McBratney, A. B., Minasny B., 2010. Proximal soil sensing. Spinger
492 Netherland, 448 p.
493 Zhang Z., Oldenburg D. W., 1999. Simultaneous reconstruction of 1-D susceptibility and
494 conductivity from electromagnetic data. Geophysics, 64-1, 33-47.

Appendix I Characteristics of the devices used for field studies

SH3: this apparatus is a laboratory prototype designed in 1977 (Parchas and Tabbagh 1978). It has a PARA coil orientation (the two coils have parallel axes aligned at 35° from the vertical, such that their direct coupling is null in free space), a 1.5 m coil separation, a coil center height of d=0.2 m, and is operated at 8.04 kHz.

CMD: this apparatus is a multi-receiver EMI (Gf Instruments, Ltd, Brno) comprising one transmitter coil and three receiver coils, located at distances of 0.32, 0.71 and 1.18 m from the transmitter. All the coils are coplanar, allowing the instrument to be used in either HCP or VCP configurations. The instrument's operating frequency is 30 kHz, and it can be used in a continuous recording mode by a mobile operator in the field, with an above-ground clearance of d=0.12 m.

DualEM 421S: this apparatus is a multi-receiver EMI (DualEM Ltd, Milton) operated at 9 kHz. It associates one horizontal transmitter loop with three pairs of receivers. In each pair, the first receiver is horizontal, allowing HCP measurements to be made. By rotating the entire apparatus, VCP configuration measurements can also be made. The second receiver of each pair is oriented in a radial direction from the transmitter, allowing PERP configuration measurements to be used. The receivers of the first pair are located at respectively 1m and 1.1m from the transmitter, those of the second pair at 2m and 2.1 m, and those of the third pair at 4m and 4.1m. However, in the archaeological surveys presented here, data from the third pair were not considered. Data from the VCP 1m, VCP 2m, HCP 1m, HCP 2m, PERP 1.1m and PERP 2.1m are used in the present study.

519

520 **Figure captions**

521 Figure 1: Flowchart demonstrating the full process with both a 1D non-linear inversion and a
522 3D linear inversion over the variations.

523 Figure 2: Description of the different bodies used to generate synthetic data

524 Figure 3: Apparent magnetic susceptibility maps calculated using the method of moments and
525 the characteristics of the seven devices under consideration.

526 Figure 4: Results of the 1D inversion when three layers are considered: the first is centered at
527 z_1=0.3 m and has a thickness e_1=0.2 m, the second is centered at z_2=0.5 m and has a thickness
528 e_2=0.2 m, and the third is centered at z_3=0.8 m and has a thickness e_3=0.4 m.

529 Figure 5: Results of the 3D linear inversion when three layers are considered (using the same
530 geometries as in Fig. 3), and the norm of the $\boldsymbol{\kappa}$ vector is minimized using $\lambda=trace/2$

531 Figure 6: Balloy neolithic enclosure: (a) SH3 apparent magnetic susceptibility, the relatively
532 high level is explained by the high susceptibility of the upper layer of soil (approx. 100 x 10^{-5}
533 SI), and the inverted magnetic susceptibility of a layer situated between the depths of 0.25 m
534 and 0.65 m, derived from the 1D inversion (b) and from the 3D linear inversion (c). The
535 rectangles indicate the contour of the targeted area used for 3D non-linear inversion.

536 Figure 7: Perdika2 (Central Thessaly, Greece) magnetic map: pseudo-gradient of the vertical
537 component of the Earth's magnetic field. The area surveyed using the CMD is colored orange.

538 Figure 8: Perdika2 site, apparent magnetic susceptibility maps measured using the CMD
539 instrument.

540 Figure 9: Perdika2 site, (a) inverted magnetic susceptibility of the 0.2 – 0.7 m and 0.7 – 1.2 m
541 layers using the 1D inversion, (b) inverted magnetic susceptibility of the 0.2 – 0.7 m and 0.7 –
542 1.2 m layers using the 3D linear inversion.

543 Figure 10: Medamud site (Egypt), three apparent magnetic susceptibility maps measured
544 using the CMD instrument over the 44m x 60 m survey area.
545 Figure 11: Medamud site, (a) inverted magnetic susceptibility of the 0.05 – 0.35 m and 0.35 –
546 0.65 m layers using the 1D inversion, (b) inverted magnetic susceptibility of the 0.05 – 0.35 m
547 and 0.35 – 0.65 m layers using the 3D linear inversion. The white rectangles indicate the
548 contour of the targeted area used for 3D non-linear inversion.
549 Figure 12: Thérouanne (Pas-de-Calais, France) site, four apparent magnetic susceptibility
550 maps.
551 Figure 13: Thérouanne site, inverted magnetic susceptibility of the 0.25 – 0.75 m, 0.75 –
552 1.25 m, and 1.25 – 2.25 m layers using the 1D inversion.
553 Figure 14: Thérouanne site, inverted magnetic susceptibility of the 0.25 – 0.75 m, 0.75 –
554 1.25 m, and 1.25 – 2.25 m layers using the 3D linear inversion.
555

556

557 **Table captions**

558 Table 1: Inverted susceptibility contrast (in 10^{-5} SI) as a function of the slab's depth of the
559 slab, z, and the separation between transmitting and receiving coils, *L* (the original value
560 being 200 10^{-5} SI), (a) VCP configuration, (b) PERP configuration (the symbol X means that
561 the shape of the slab is not correctly restored and unidentifiable), (c) HCP configuration and
562 (d) PARA configuration

563

564 Table 2: Inverted susceptibility contrast when a 2m x 2m x 0.6 m body, of 200 10^{-5} Si
565 susceptibility contrast is divided into 5 thin layers of 0.12m thickness, determined using
566 respectively five, six and seven different instrumental configurations (constraint II is used in
567 the inversion).

568 Table 3: Characteristics of seven instrumental configurations used to interpret inversion
569 processes with synthetic data.

570

	L=0.5 m	*L=0.7 m*	*L=1 m*	*L=1.5 m*	*L=2 m*
z=0.3 m	195	187	153	169	153
z=0.5 m	227	224	209	226	200
z=0.7 m	245	235	221	236	234
z=1 m	242	241	239	241	229
z=1.5 m	250	226	219	249	205

571 Table 1(a)

572

	L=0.5 m	*L=0.7 m*	*L=1 m*	*L=1.5 m*	*L=2 m*
z=0.3 m	206	258	183	X	X
z=0.5 m	235	244	217	259	219
z=0.7 m	242	240	233	253	228
z=1 m	252	245	252	248I	230
z=1.5 m	X	X	X	249	193

573 Table 1(b)

574

	L=0.5 m	*L=0.7 m*	*L=1 m*	*L=1.5 m*	*L=2 m*
z=0.3 m	296	120	240	225	X
z=0.5 m	271	221	215	233	302
z=0.7 m	266	304	257	224	284
z=1 m	271	282	263	292	276
z=1.5 m	277	279	249	280	248

575 Table 1(c)

576

	L=0.5 m	*L=0.7 m*	*L=1 m*	*L=1.5 m*	*L=2 m*
z=0.3 m	217	205	185	222	224
z=0.5 m	318	247	249	255	241
z=0.7 m	289	280	258	272	276
z=1 m	280	287	260	283	275
z=1.5 m	273	277	179	311	284

577 Table 1(d)

578

579

Different instrument configurations used	Inverted susceptibility contrast (x 10^{-5} SI) for 5 layers
5 configurations : PERP 1 m, PERP 1.5 m, VCP 0.7 m, VCP 1 m and PARA 1.5 m	Layer 1 (centered et 0.26m) 219.5 Layer 2 (centered at 0.38 m) 219.8 Layer 3 (centered at 0.50 m) 220.2 Layer 4 (centered at 0.62 m) 220.4 Layer 5 (centered at 0.74 m) 220.5
6 configurations : PERP 0.7 m, PERP 1 m, PERP 1.5 m, VCP 0.7 m, VCP 1 m and PARA 1.5 m	Layer 1 217.6 Layer 2 218.0 Layer 3 218.3 Layer 4 218.5 Layer 5 218.6
7 configurations : PERP 0.7 m, PERP 1 m, PERP 1.5 m, VCP 0.7 m, VCP 1 m, VCP 1.5 m and PARA 1.5 m	Layer 1 219.1 Layer 2 219.5 Layer 3 219.8 Layer 4 220.4 Layer 5 220.5

580 Table 2

581

582

583

Apparatus	Geometrical configuration	Inter-coil separation (m)	Frequency (kHz)	Height of the coils (m)
SH3	PARA	1.5	8.0	0.2
PRP6	PERP	0.6		
PRP10	PERP	1.0		
PRP15	PERP	1.5		
VCP6	VCP	0.6		
VCP10	VCP	1.0		
VCP15	VCP	1.5		

584 Table 3

585

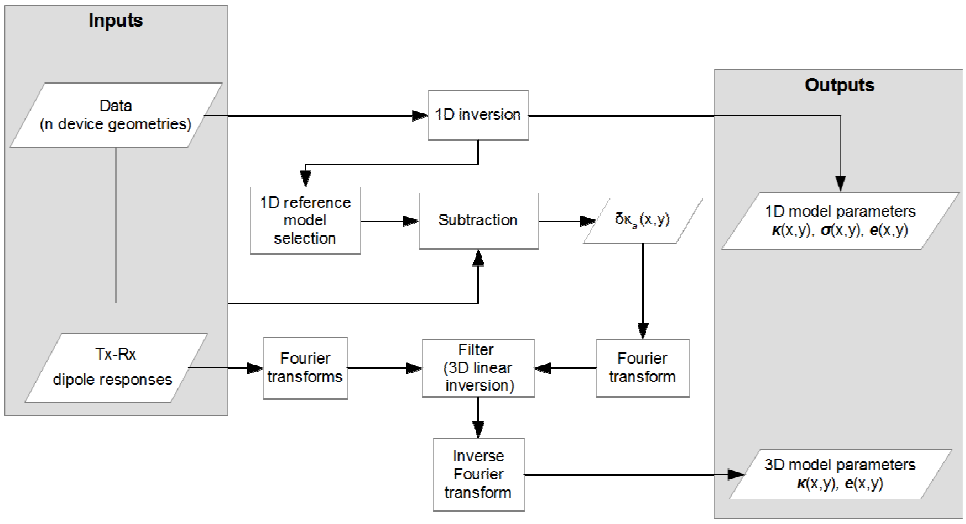

586

587 Fig. 1

588

589

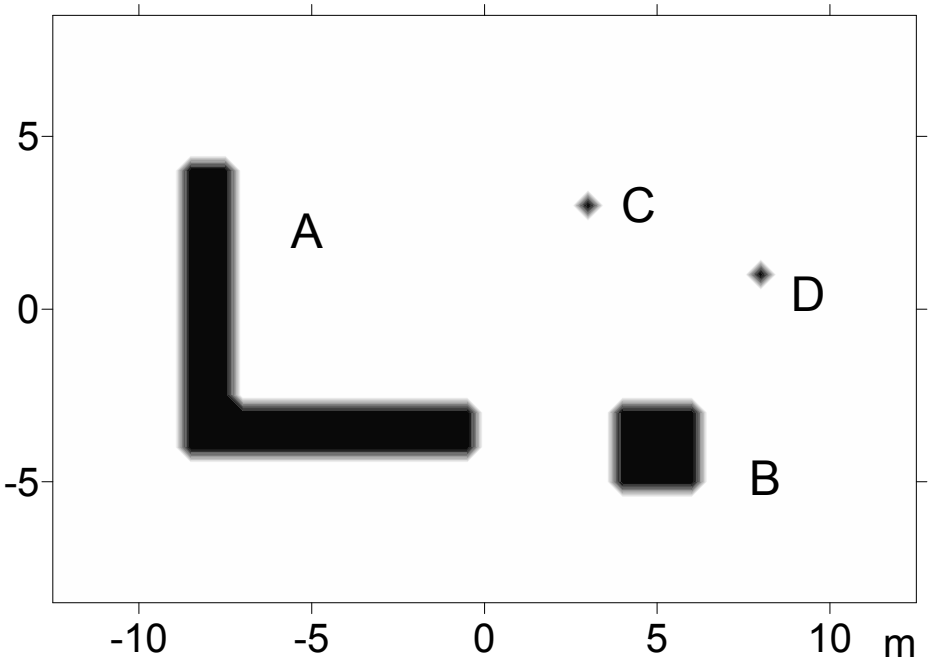

590

591 Fig. 2

592

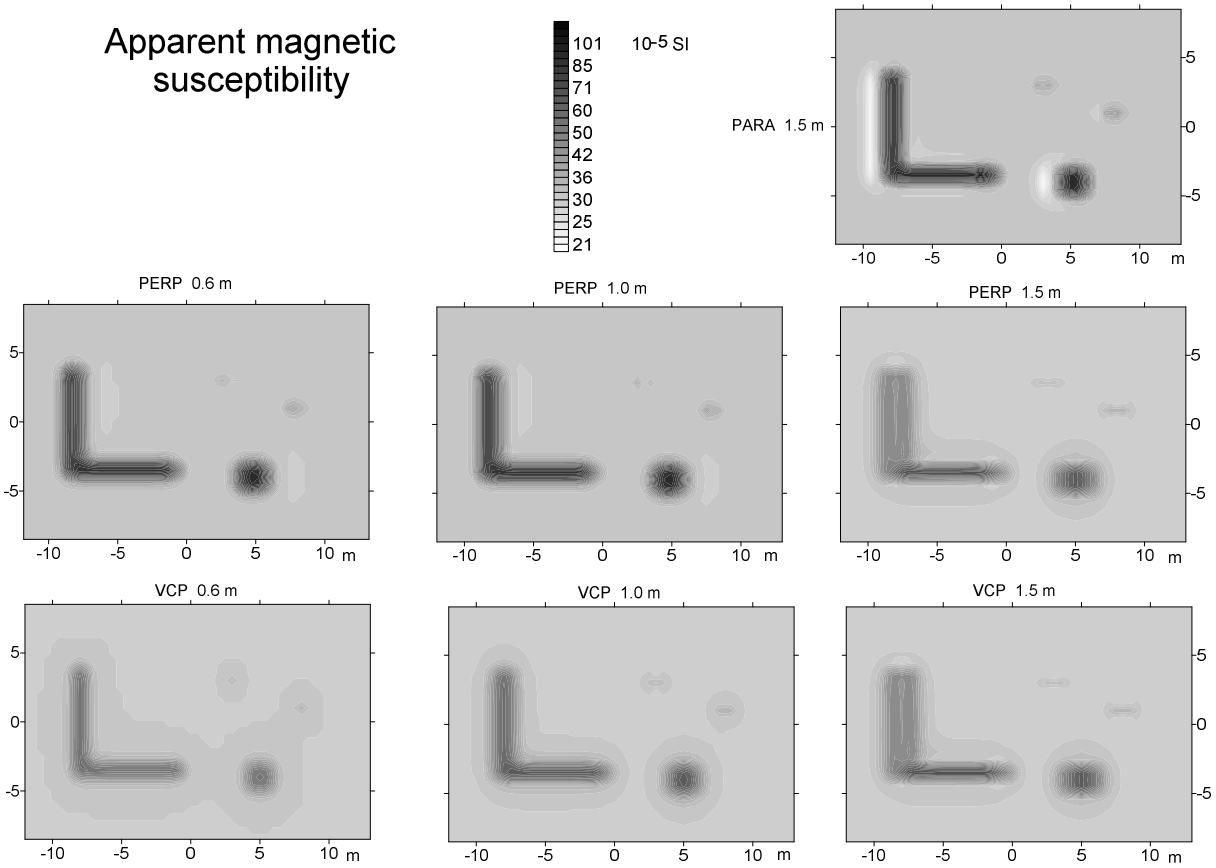

593

594 Fig. 3

595

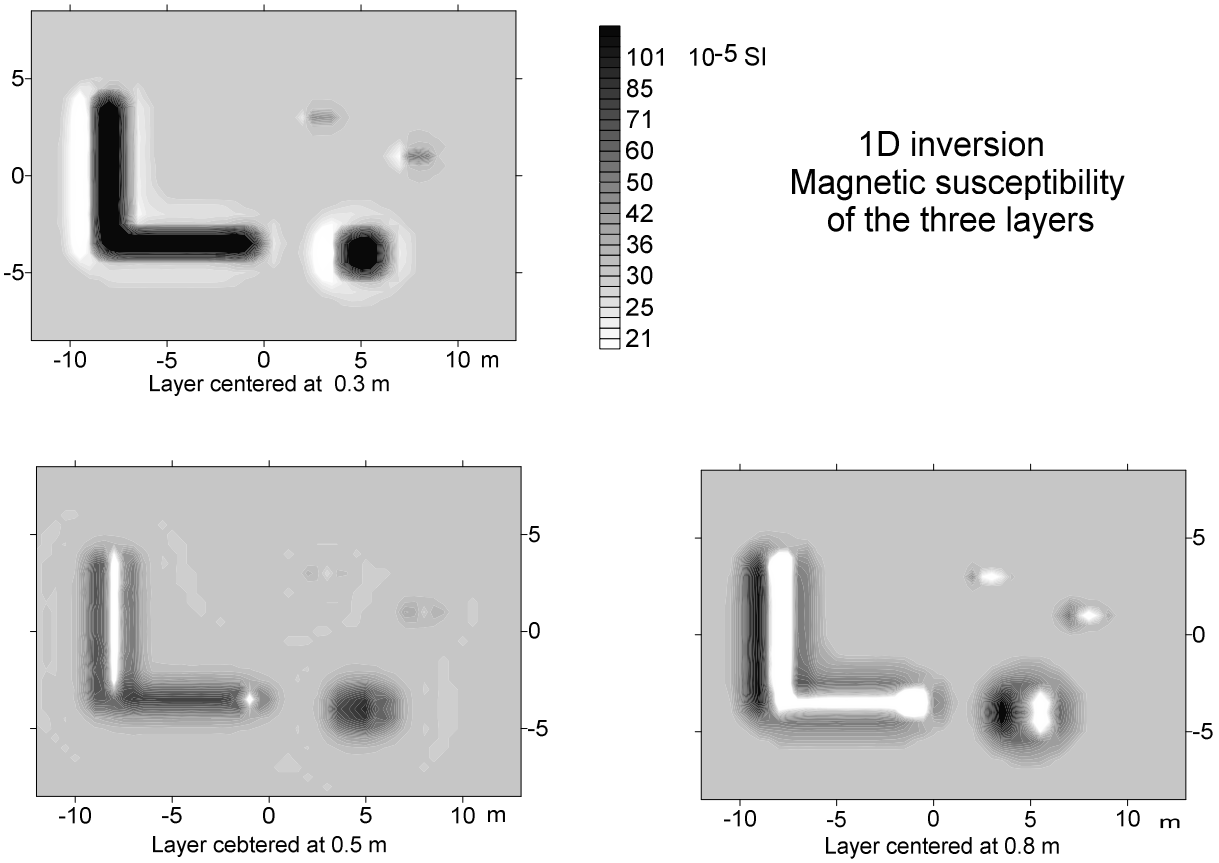

596

597 Fig. 4

598

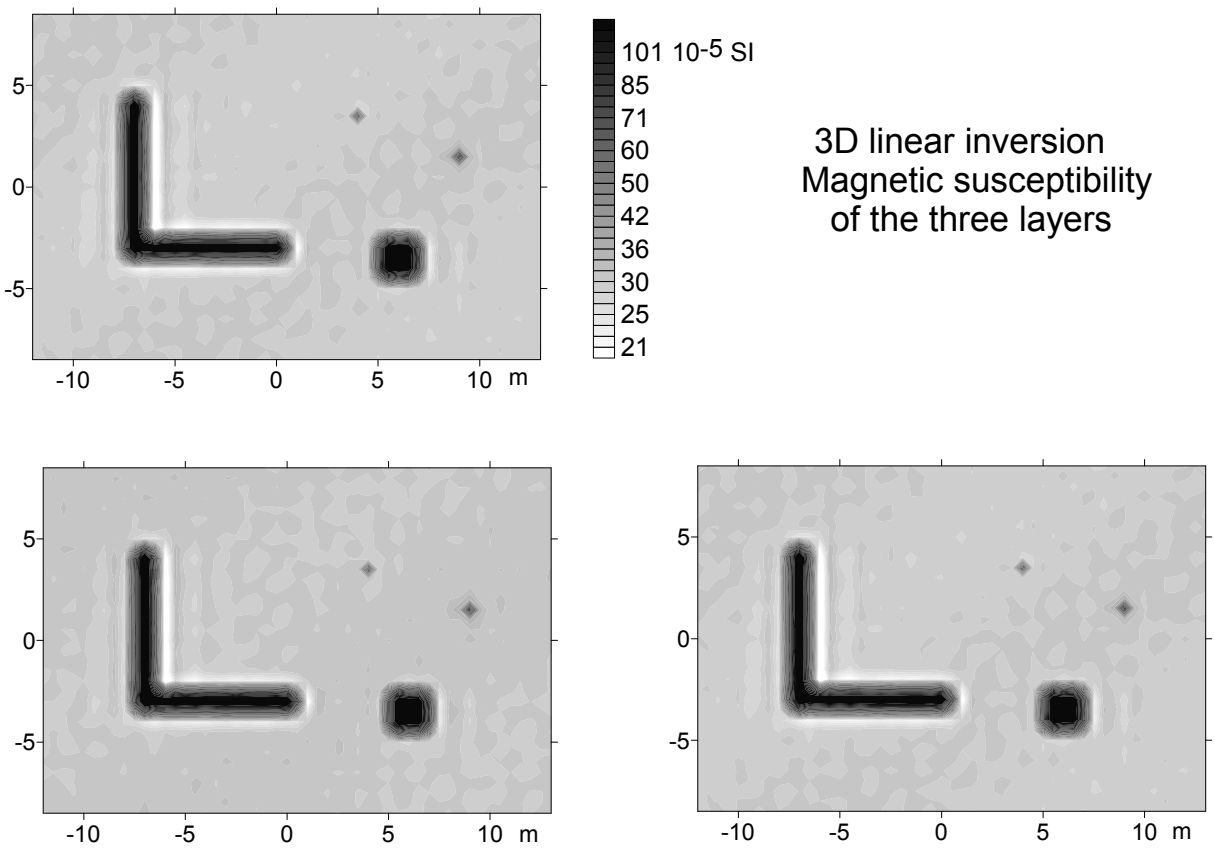

599

600 Fig. 5

601

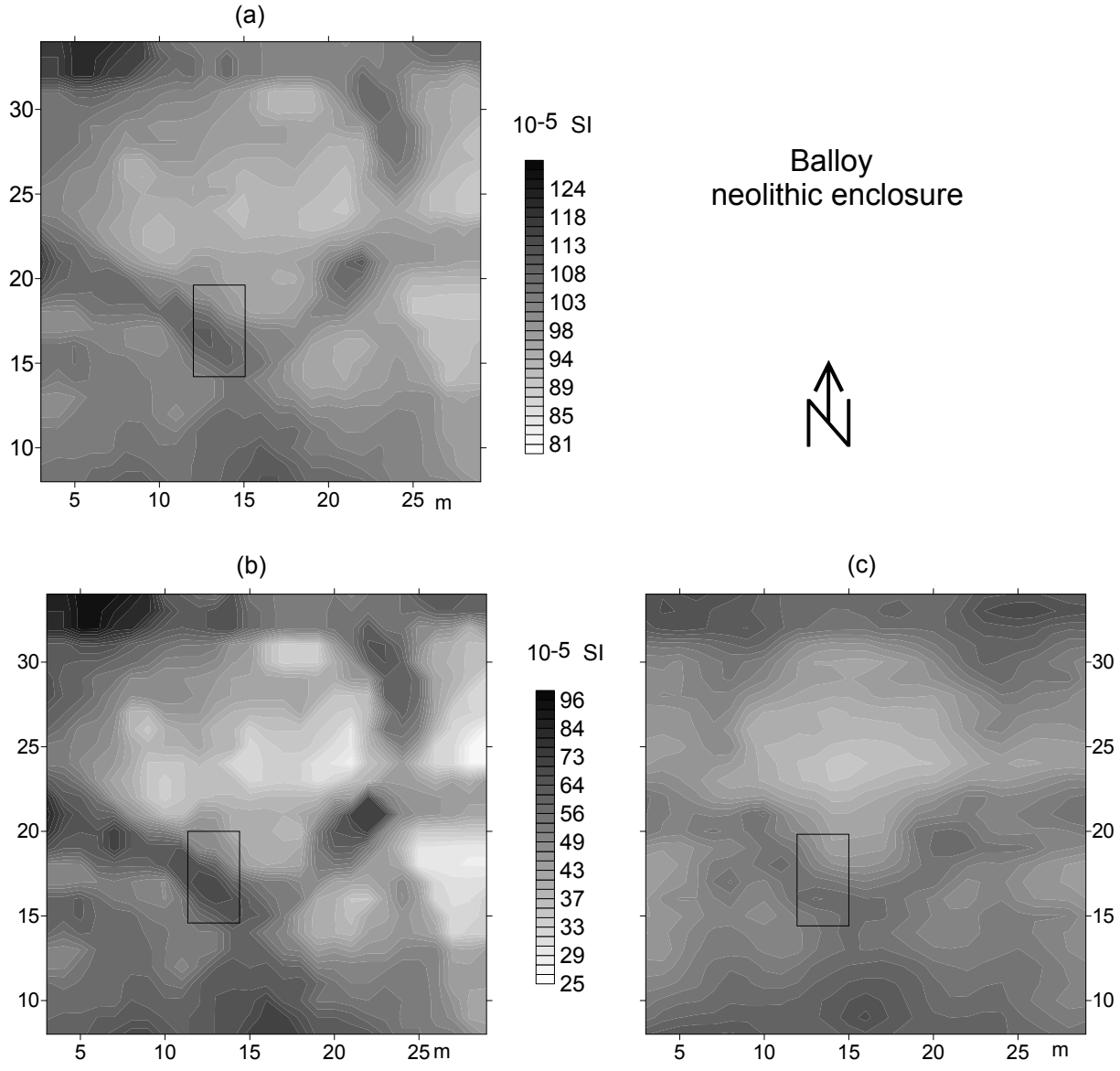

602

603 Fig. 6

604

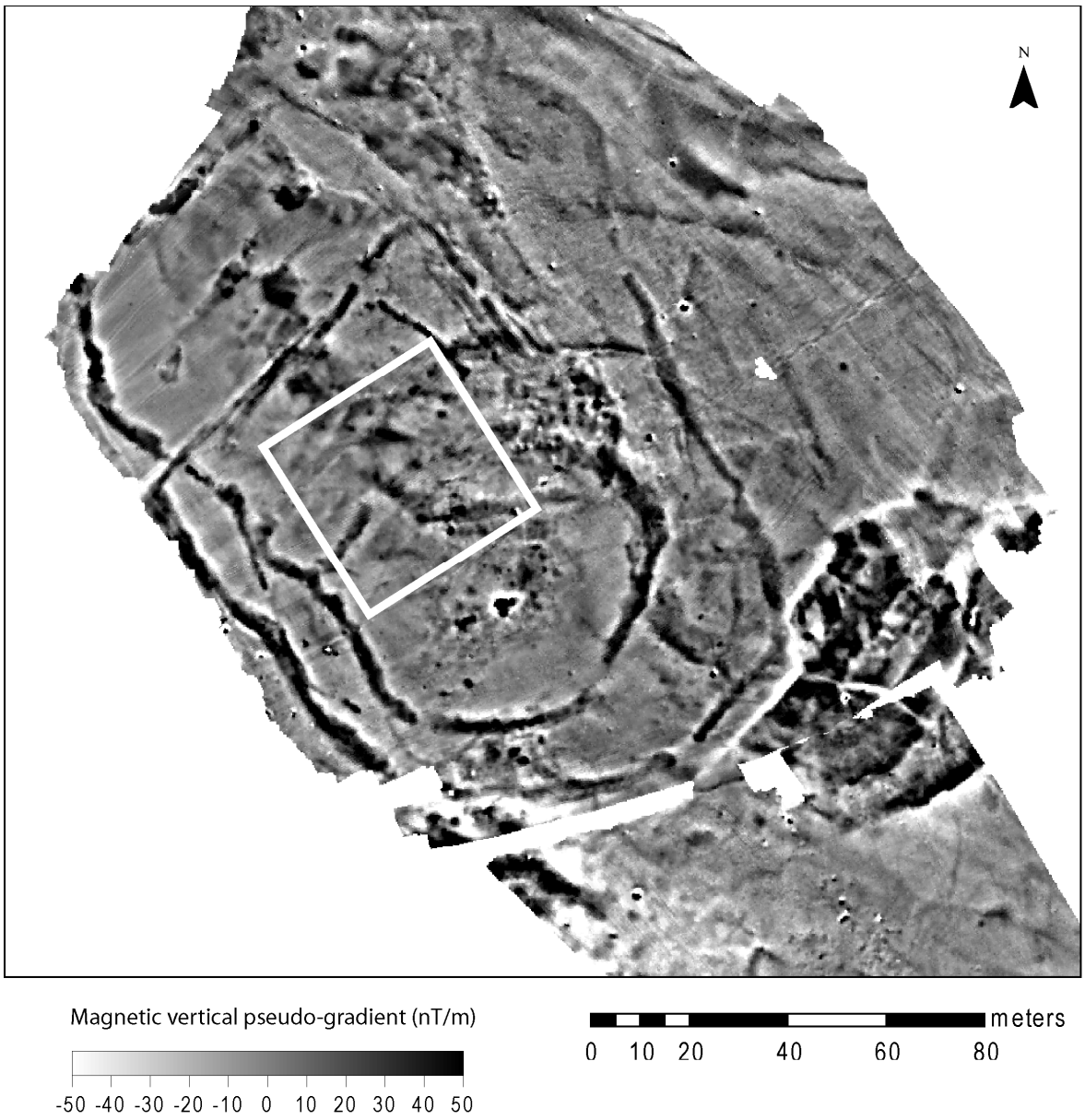

605

606 Fig. 7

607

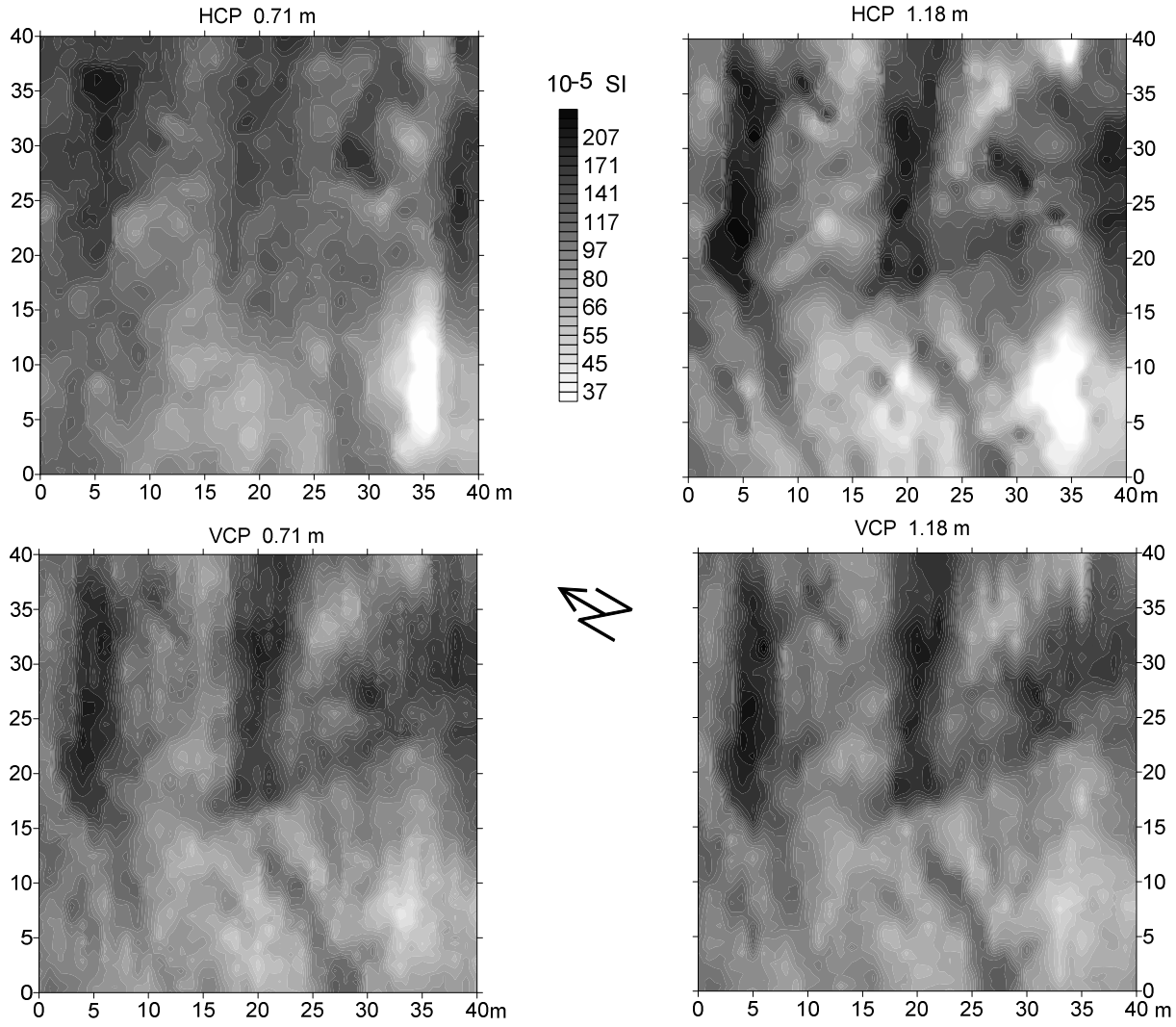
HCP 0.71 m
HCP 1.18 m
VCP 0.71 m
VCP 1.18 m
10-5 SI
207
171
141
117
97
80
66
55
45
37
0 5 10 15 20 25 30 35 40 m
N

Fig. 8

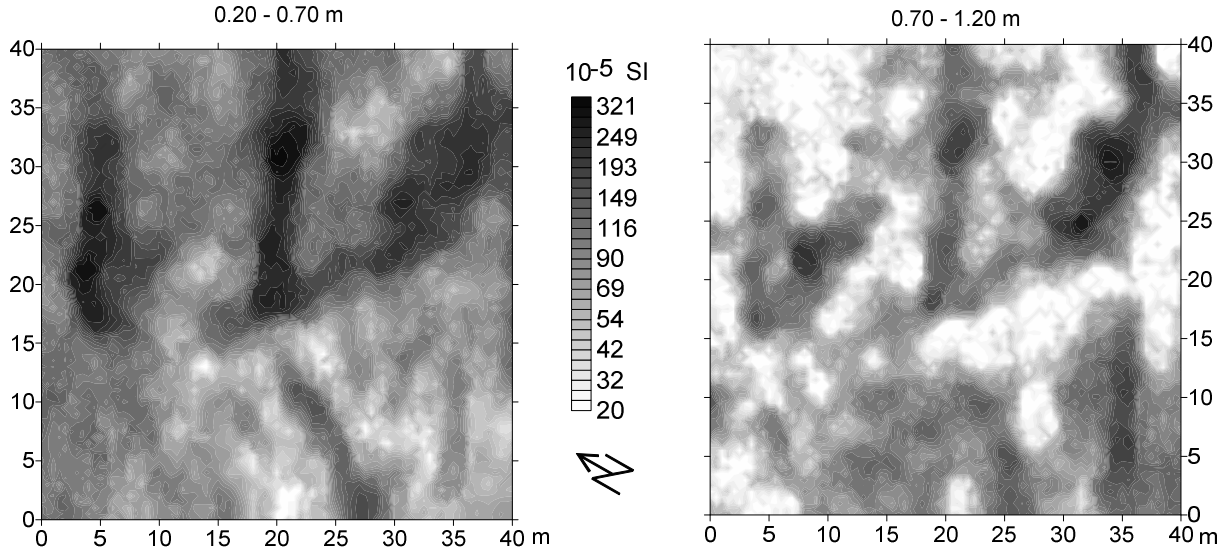
0.20 - 0.70 m
0.70 - 1.20 m
10-5 SI
321
249
193
149
116
90
69
54
42
32
20
0 5 10 15 20 25 30 35 40 m

Fig. 9a

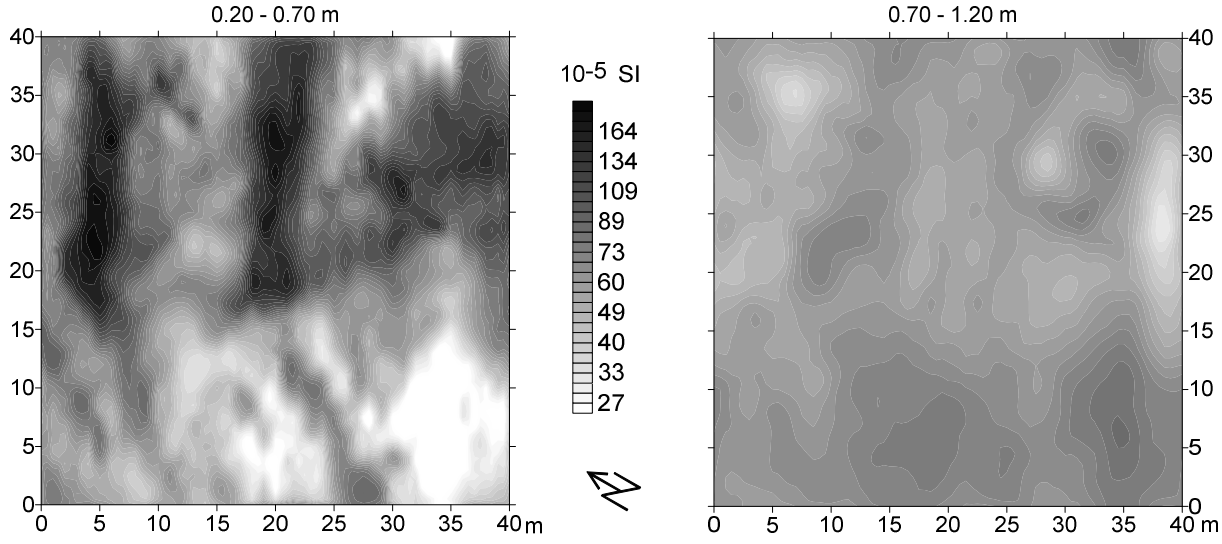
0.20 - 0.70 m
0.70 - 1.20 m
10-5 SI
164
134
109
89
73
60
49
40
33
27
0 5 10 15 20 25 30 35 40 m

Fig. 9b

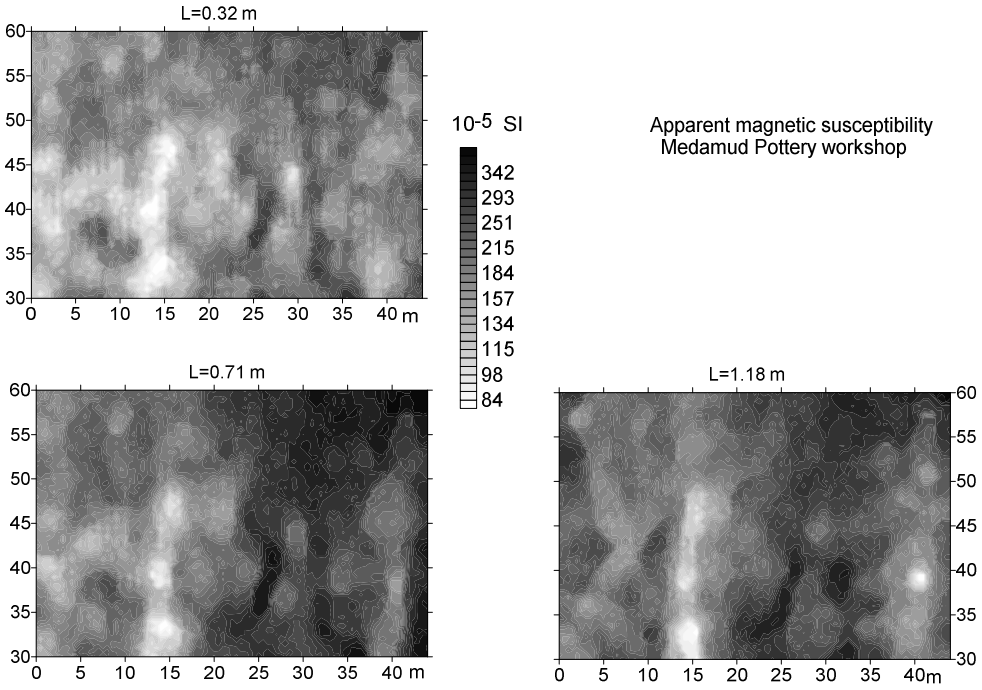

617

618 Fig. 10

619

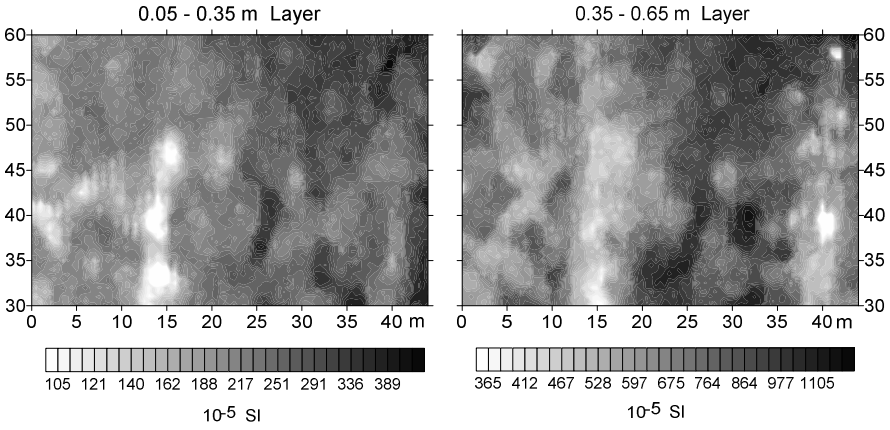

620

621 Fig. 11a

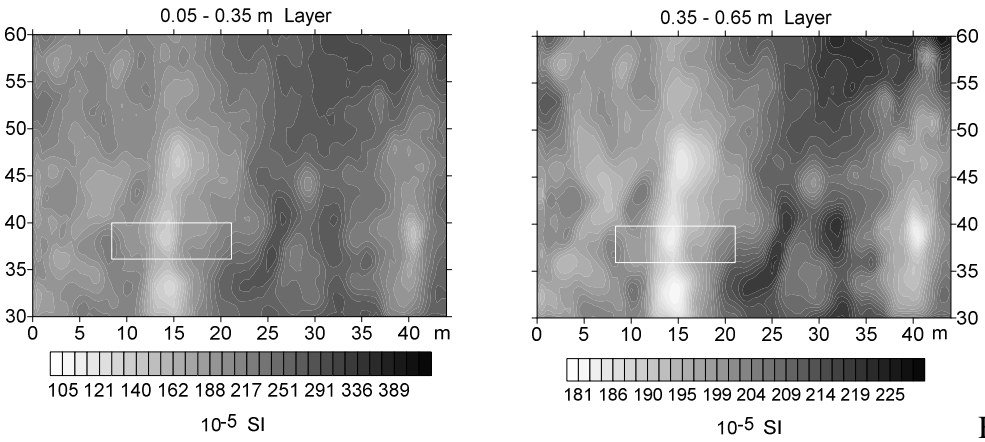

622 Fig. 11b

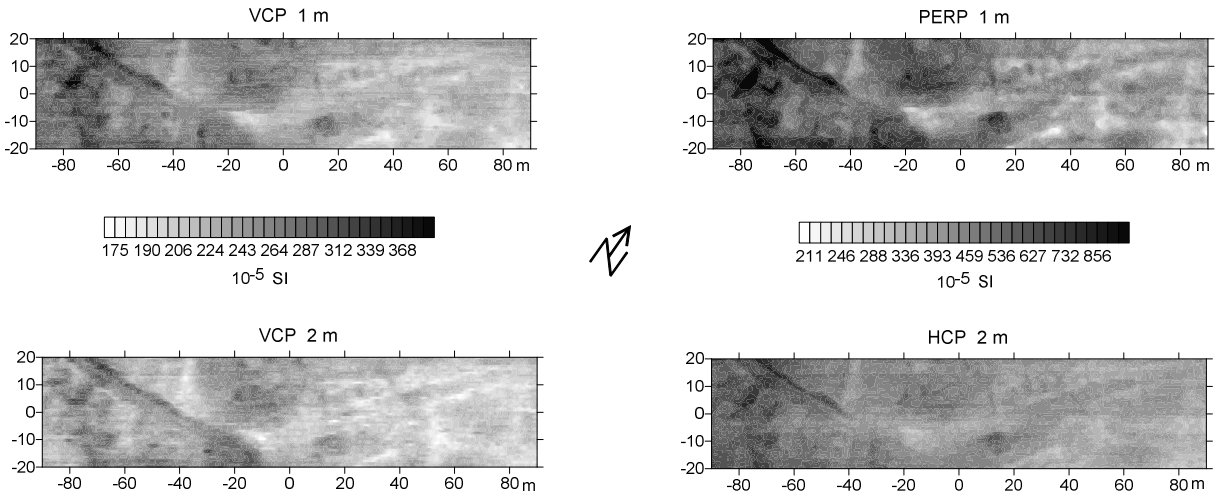

623

624 Fig. 12

625

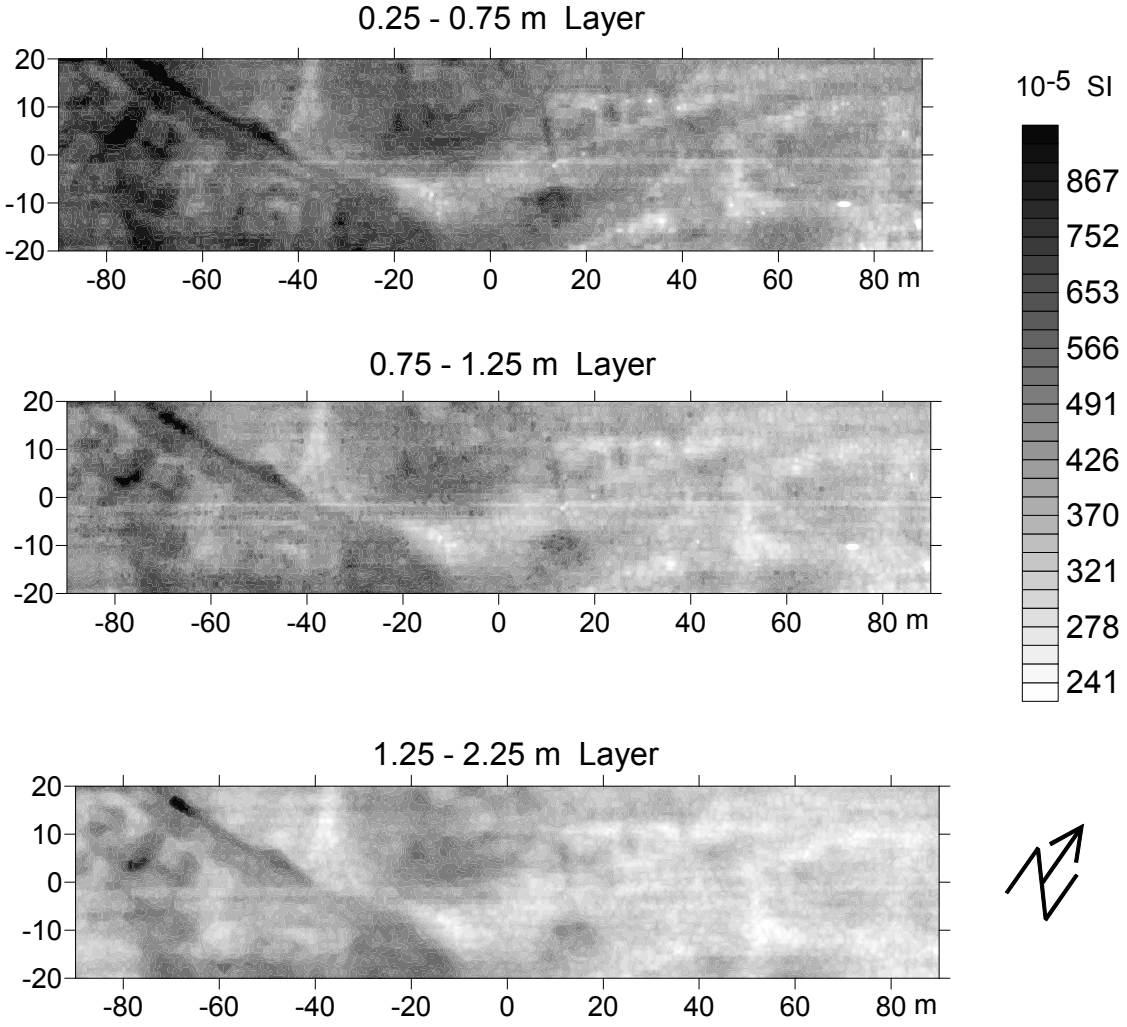

626

627 Fig. 13

628

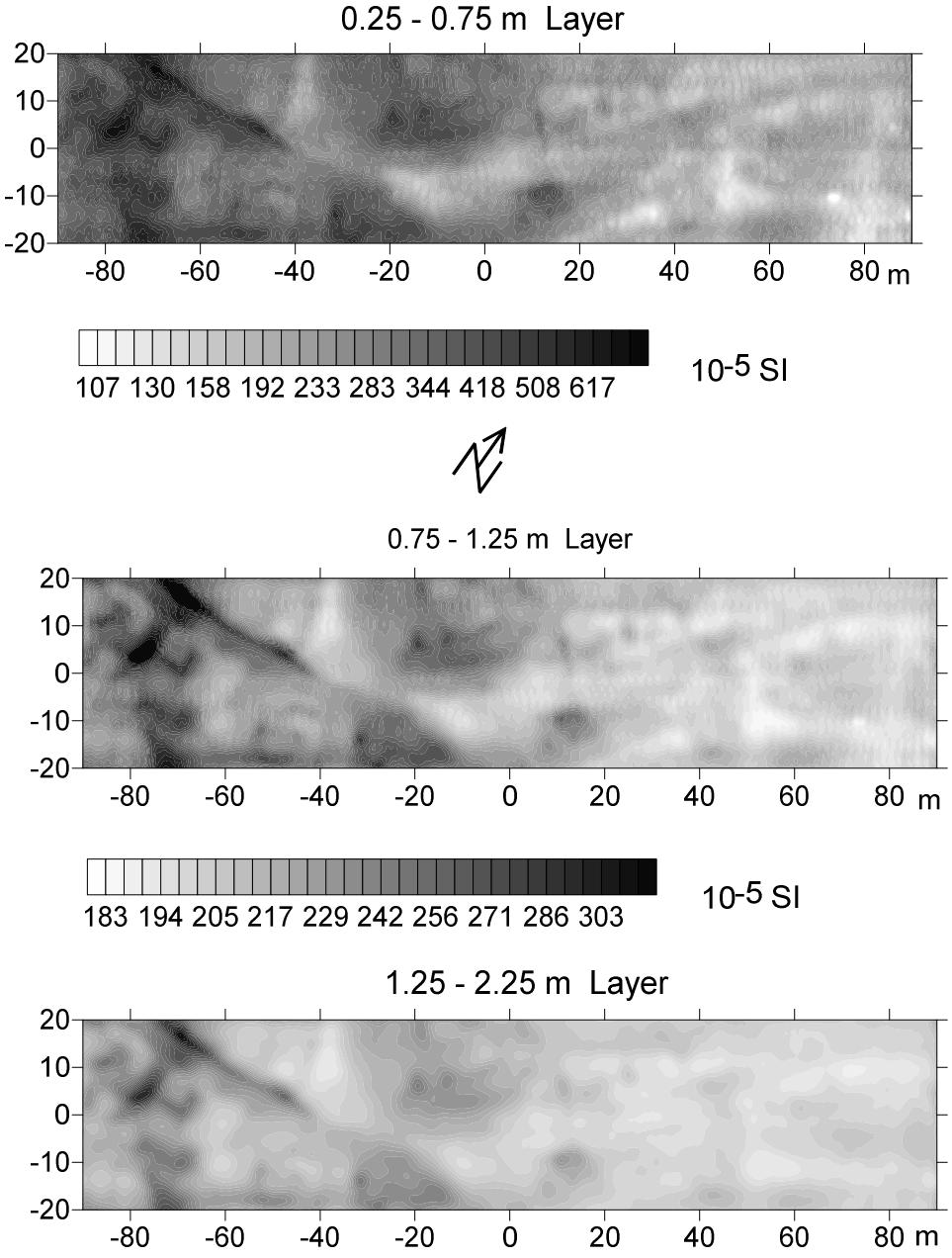

629

630 Fig. 14